Proceedings of the 21st ICSMGE, Vienna, Austria, 14 – 19 June 2026. Pistrol, Adam & Schweiger (eds.)
Published by: ÖGG, Austrian Society for Geomechanics, Salzburg, Austria, ISBN 978-3-9503898-4-5
https://doi.org/10.53243/ICSMGE2026-469

Impact of 3D seismic soil-foundation-structure interaction on damage and settlement patterns of a masonry tower in southern Italy

Onur Deniz Akan, Guido Camata, Enrico Spacone
Department of Engineering and Geology, University of Chieti-Pescara, Pescara, Italy,
onurdeniz.akan@unich.it

Carlo G. Lai
Department of Civil Engineering and Architecture, University of Pavia, Pavia, Italy

Claudio Tamagnini
Department of Civil and Environmental Engineering, University of Perugia, Perugia, Italy

ABSTRACT: Soil-foundation-structure interaction (SFSI) plays a critical role in the seismic performance of masonry towers. This study investigates the relationship between foundation deformations and structural cracking, focusing on hysteretic energy dissipation mechanisms within the SFSI of shallow-founded masonry towers located on fine-grained soils. A virtual SFSI laboratory has been developed using OpenSees and the Scientific Toolkit for OpenSees (STKO) pre-processor, incorporating a finite element digital twin of the St. Maria Maggiore Cathedral's bell tower in Guardiagrele. The model includes the adjacent cathedral walls and the stratified subsoil. The masonry components, the foundation system, and the soil are modelled utilizing 8-node brick elements. The fine-grained soil response is modelled using a pressure-independent multi-yield model, whereas the masonry behavior is idealized through a damage-plasticity material model capturing crack formation The model has an average depth of 51.4 m and comprises about 220,000 finite elements. A set of three-component ground motions is applied at the base of the model to assess the seismic response of the SFSI system due to vertically propagating waves with a frequency content ranging up to 18 Hz. The ground motions were selected to match the conditional spectrum conditioned on average spectral acceleration expected at the site for a 475-year return period. The analysis reveals that foundation rotations can reduce the seismic demand on the tower, demonstrating a trade-off between foundation compliance and structural damage. The soil shear modulus reduction curves beneath the foundation are a key driver of this behavior. Additionally, cracking in the foundation masonry during seismic shaking significantly contributes to the permanent settlement of the tower. These findings underscore the importance of accurately modelling nonlinear material behavior in both soil and masonry to better understand the seismic response of masonry towers.

KEYWORDS: Masonry tower, Seismic assessment, Soil-structure interaction (SSI), Cracking damage, Permanent settlement.

1 INTRODUCTION

Unreinforced masonry (URM) towers are part of the historical heritage and were often constructed as security structures or bell towers during the Renaissance period. They can be found as standalone edifices or as components of larger architectural complexes. The inherent brittleness of masonry renders tower structures particularly hazardous, as collapses can occur without warning and lead to catastrophic results.

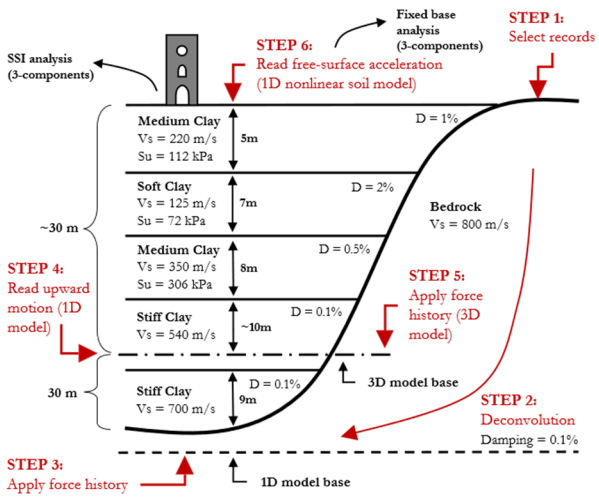

Figure 1. Illustration of the 1D ground response problem considered ensuring that the accelerations acting on the tower during the SSI and fixed-base analyses are compatible.

The flexibility of the masonry foundation and the energy dissipation provided by the hysteretic response are essential factors in assessing seismic performance. Kinematic interaction, meaning the mismatch between the stiffness of the foundation and that of the surrounding soil, can cause wave scattering and diffraction, which may significantly influence the structural response. At the same time, aspects of wave propagation, such as the frequency dependent wave amplitude, affect how the shaking develops at the foundation level. Depending on the soil profile and stiffness, the accelerations transmitted to the foundation may be amplified or reduced.

The mechanisms that lead to the damage and collapse of masonry towers remain an open research question. They require the study of complex material, geometric, and interaction nonlinearities. Over the years, numerical investigation of various URM tower systems has received increasing attention from researchers (Camata et al., 2008; Rosell, 2010; Milani and Clementi, 2021; Romero-Sánchez et al, 2024). The modelling of direct soil–structure interaction (SSI) for large structures and the influence of foundation aspect ratio (Dashti et al., 2010; Bray and Macedo, 2017; Bullock et al., 2019), indicates that SSI effects can significantly alter the response of stiff structures due to soil amplification, kinematic effects, or the inertial response of a heavy oscillating body.

The work of Gazetas and co-authors (Anastasopoulos et al., 2011; Gelagoti et al., 2012; Gazetas, 2015) provides detailed insight into how soil–foundation–structure interaction can be managed in seismic analysis. Their studies on reinforced concrete (RC) frames have shown that allowing controlled foundation rocking during seismic events can be beneficial. This rocking isolation dissipates energy through foundation motion and reduces the forces transmitted to the superstructure.

The improved seismic resilience observed in these studies suggests that similar mechanisms could also influence the seismic demands acting on masonry towers.

This study focuses on the combined effect of cyclic damage–plasticity behavior in masonry structures, such as period shift, and stiffness reduction in foundation on the overall seismic response. A high-fidelity numerical model is developed in OpenSees with the aid of the STKO pre-processor (Petracca et al., 2017). The model represents the bell tower and cathedral of Guardiagrele along with the underlying stratified soil profile extending to the bedrock. Nonlinear material characteristics are assigned to both the masonry and the soil, and the pounding interaction between the bell tower and the church walls is explicitly modelled. To enable the simulation of these complex interactions, a novel IMPL-EX contact element and an IMPL-EX version of the pressure-independent soil material are implemented in OpenSees.

The methodology also incorporates a ground motion selection process designed to ensure consistent input for both the direct SSI and fixed-base models. This is achieved through nonlinear one-dimensional site response analysis, which adjusts the input motions so that the accelerations at the tower's base are compatible in both modelling approaches. Figure 1 outlines this process, from the selection of earthquake records to their deconvolution to the model base, and their subsequent application in the one-dimensional and three-dimensional soil analyses.

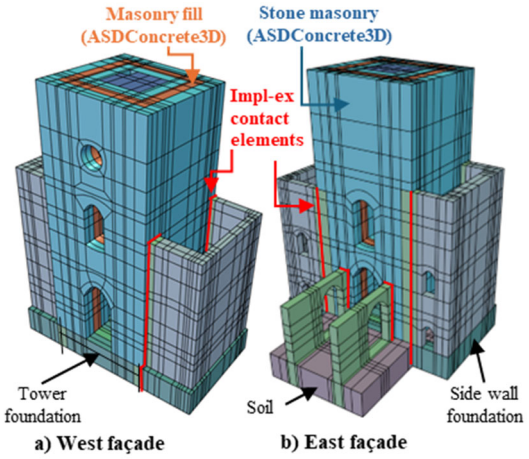

Figure 2. The spatial distribution of material properties in the FE model of the bell tower of Guardiagrele.

2 FINITE ELEMENT MODELING IN OPENSEES

The structure is modeled using 8-node brick solid elements. It is represented as four separate bodies: the bell tower, the north church wall, the south church wall, and the rear church wall. Contact between these components is defined using node-to-node ZeroLengthContactASDimplex elements (Figure 2). These elements reproduce two key behaviors during seismic shaking. The first is contact and separation, which allows simulation of pounding or opening at the interfaces between the tower and adjacent walls. The second is stick–slip behavior, which governs sliding once contact is re-established. A stable IMPL-EX Mohr–Coulomb law (Oliver et al., 2008; Akan, 2024) is adopted for these contact interfaces to ensure realistic representation of frictional resistance and slip throughout the analysis.

Figure 3 shows the calibration of the ASDConcrete3D material model (Petracca et al., 2022), which is used for both the stone masonry and the fill materials. This model includes tension–compression damage, fracture energy regularization, and IMPL-EX integration. The finite element representation also accounts for the influence of mortar joints within the masonry by adopting an orthotropic failure criterion (Pelà et al., 2013). This orthotropic formulation is crucial for reproducing diagonal cracking and shear banding modes observed in experiments. The model is calibrated against the results of a cyclic stone masonry shear wall test conducted at Eucentre by Guerrini et al. (2017). This calibration ensures that the numerical model realistically captures the energy dissipation mechanisms under dynamic seismic loading (Akan, 2024).

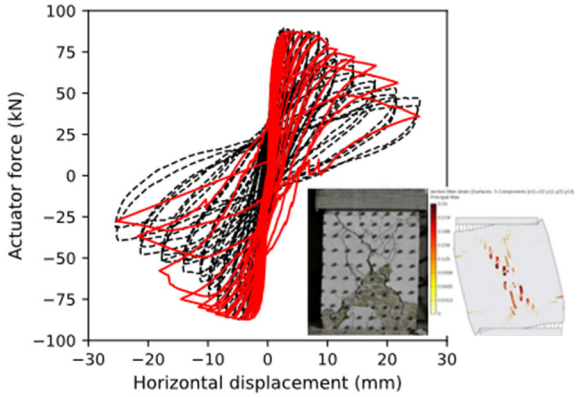

Figure 3. ASDConcrete3D model calibration to match cyclic test.

The site stratigraphy consists mainly of fine-grained soils, predominantly clays and silty clays with a moderate Plasticity Index (PI ≈ 15). The shear wave velocity profile (Figure 5), V_s, along with the soil stratification, is determined from site investigations. The undrained shear strength of each layer is calculated as a linear function of the small-strain shear modulus, following the calibration method of Anastasopoulos et al. (2011). The backbone stress–strain relationship is adjusted to match the shear modulus reduction curves proposed by Vucetic and Dobry (1991). The soil behavior is simulated using the kinematic hardening Pressure-Independent Multi-Yield (PIMY) material model (Mróz, 1967; Prevost, 1989; Gu et al., 2011), which captures cyclic plasticity and stiffness degradation in fine-grained soils.

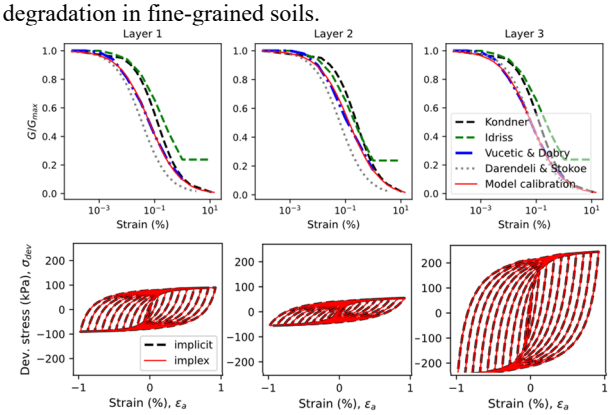

Figure 4. Pressure-independent model calibration to match G/Gmax backbone proposed by Vucetic and Dobry (1991) for clayey soils.

Finally, the mesh size at the structure level is approximately 0.5 m, providing adequate resolution for the structural modes of interest. The soil mesh is refined to capture vertically propagating waves with a maximum frequency of 18 Hz. In the transition zone around the foundation, the brick elements are sized at 1×1×1m to avoid numerical size effects. The structural and soil meshes, which have different densities, are connected using ASDEmbeddedNode elements. The

complete model contains about 220,000 elements and is solved in parallel using 24 partitions in OpenSeesMP (Figure 6).

3 DESIGN LEVEL GROUND MOTION SET SELECTION

The input ground motion should accurately model the site's seismic hazard and seismotectonic characteristics. Since the finite element (FE) model is designed to simulate the dynamic response from the bedrock to the structure, selecting a hazard-consistent strong motion set representing the incident wave at the model's base is essential. Following the approach illustrated in Figure 1, all ground motions are treated as if recorded at an outcropping bedrock site located at the tower. Each record is then deconvolved to obtain the within motion at the depth corresponding to the FE model base. This process ensures that hazard consistency is established at the outcropping bedrock level, then translated to the model base.

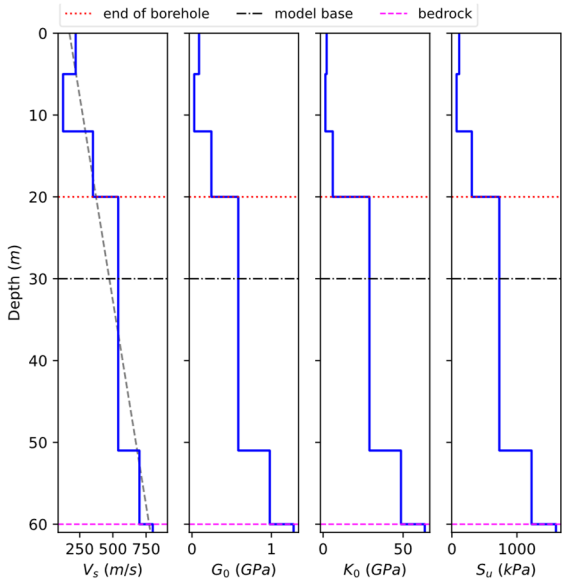

Figure 5. Site profile adopted in the analyses: depth variation of V_s, G_0, K_0, and S_u. Horizontal markers denote the end of borehole, the FE model base, and the bedrock level.

In Figure 7, a set of eleven ground motions is selected so that their mean response spectrum matches the target spectrum, and their dispersion is consistent with the hazard model (Whittaker et al., 2011). The record selection is performed using the conditional spectrum (CS) tools available in the EzGM library (Ozsarac et al., 2023), with hazard inputs from the OpenQuake engine (Pagani et al., 2014), and the SHARE model for continental Europe (Woessner et al., 2015). The target intensity measure, AvgSA, is defined as the geometric mean of spectral accelerations from 0.1-to-1.0s in 0.1s intervals (Kohrangi et al., 2017).

A disaggregation analysis is done to identify the significant magnitude (M), distance (R), and epsilon values. Then, the conditional spectrum for AvgSA is determined for a 475-year return period. The GMM by (Boore et al., 2014) is utilized to generate the conditional spectrum. Subsequently, eleven ground motion records are selected based on relevant magnitudes, distances, faulting mechanisms, and Vs30 values (> 800 m/s) from the NGA West 2 database (Ancheta et al., 2014). Reverse and strike-slip faulting mechanisms are expected based on the seismotectonic of the region (Kastelic et al., 2013). Finally, the strong motions are scaled (Maximum scaling factor = 3) at the AvgSA to match, on average, the conditional spectrum and the target dispersion.

4 THE GOVERNING DEFORMATION MECHANCISM IN SOIL-STRUCTURE INTERACTION

The acceleration history at the roof is examined using a single input motion with frequency content sufficient to drive the structure into nonlinear response. Here, the RSN4312 UMBRIA.P I-GBB record is used to compare the mechanical response of the tower under different modelling assumptions.

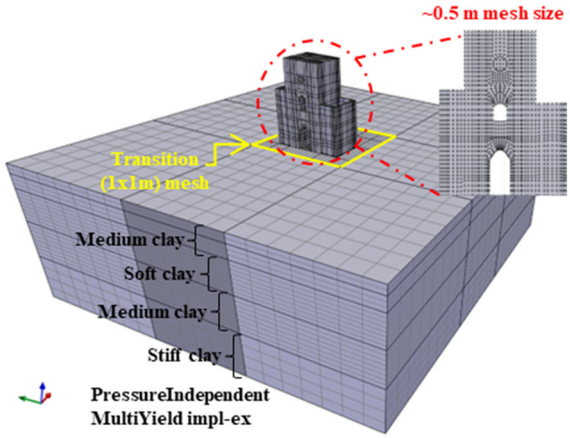

Figure 6. The soil-structure interaction model in STKO/OpenSees.

Figure 8 compares the tower's response under fixed-base (no soil) and direct SSI conditions for the same bedrock-level motion. In the fixed-base model, the corresponding free-surface motion from the 1D soil column is applied directly at the base. Both models use the three motion components, and linear analyses follow the same procedure with motions from a linear 1D site response. In the linear elastic case, the acceleration patterns differ significantly: SSI response is dominated by foundation rotation, whereas the fixed-base response is controlled by the first structural mode. Fundamental periods in the EW direction are 0.29 s (fixed) and 0.44 s (SSI), the latter due to elastic foundation rocking.

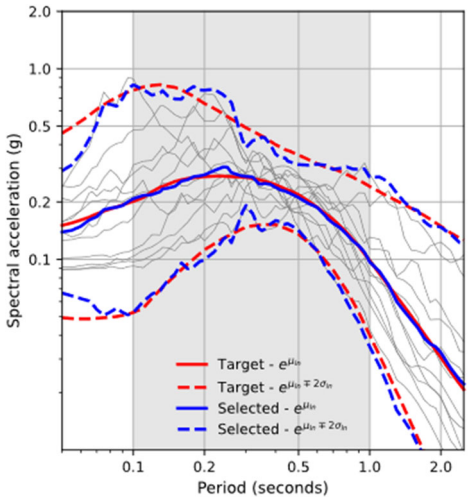

Figure 7. The selected record set. The mean AvgSA spectrum and the dispersion of the set matches the target AvgSA spectrum calculated at the site [AvgSA: 0.1-to-1.0s with 0.1s intervals].

Foundation rotation, θ, can be evaluated using two independent approaches (Figure 9). The first computes θ from vertical displacements at the foundation edges; the second estimates θ by dividing the horizontal roof displacement by the tower height (roof drift ratio, RDR). For a rigid body, RDR ≈ tan θ ≈ θ for small angles. The significant correlation between

the two rotation angles indicates that roof displacements strongly depend on foundation rotations.

Including tower flexibility gives RDR ≈ θ + φ, where φ is the deformation contribution, explains the contribution of structural modes in the roof displacements. The larger rotation values obtained through the rigid body rotation calculation reflect structural flexibility, yet the time history follows the foundation rotation pattern. It is worth noting that, early in the motion, shaking is too weak to induce notable structural deformation, so the response is almost pure rigid-body rotation.

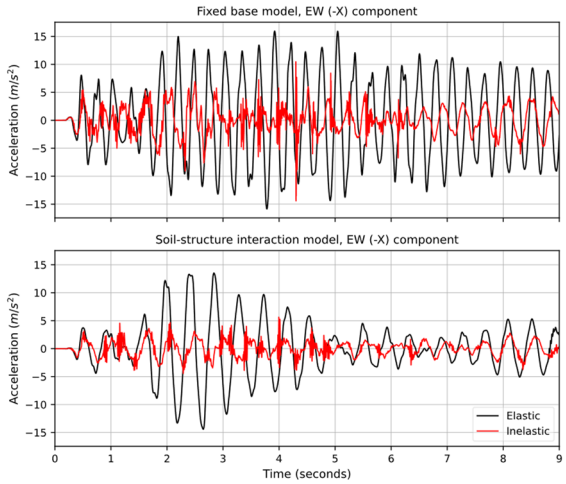

Figure 8. Roof acceleration histories for fixed-base (top) and SSI (bottom) models under the RSN4312 UMBRIA.P I-GBB record, EW component. Black: elastic; red: inelastic.

Fourier analyses of the roof acceleration histories (not shown) confirm these observations. In the fixed-base model, peaks align with the modal fundamental frequency; as nonlinearity develops, the frequency shifts, indicating period elongation in the masonry. Inelastic effects are greater in the NS direction due to openings, leading to a pronounced cracking mechanism.

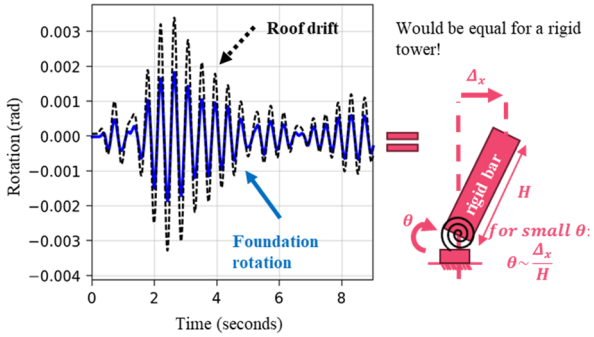

Figure 9. Foundation rotation from displacement measurements (blue) and roof drift ratio (black). Schematic shows rigid-body relation for small angles.

These results show that foundation rotation can govern both the global response and damage development. Neglecting SSI by relying on fixed-base analysis may therefore lead to inaccurate estimates of engineering demand parameters (EDPs).

5 Effect of foundation soil nonlinearity on the masonry damage pattern

Foundation soil nonlinearity can reduce structural demand by dissipating seismic energy, as noted in previous studies (Anastasopoulos et al., 2011; Gelagoti et al., 2012; Gazetas, 2015). The undrained strength (*Su*) and the *G/Gmax* degradation of the soil surrounding the foundation may affect the transfer of high-frequency accelerations to the superstructure. In return this can reduce or increase the cracking damage obtained in the masonry tower as a result of strong shaking.

To investigate, the strength and stiffness reduction characteristics of the foundation soil was varied while keeping the behavior of deeper layers constant. Figure 10 shows the stress–strain curves used, with the 110 kPa case as reference. Lower Su curves (80 kPa, 50 kPa) were obtained by reducing γ_peak in the hyperbolic equation. The hyperbolic stiffness reduction law (Kondner, 1963) was also included for comparison.

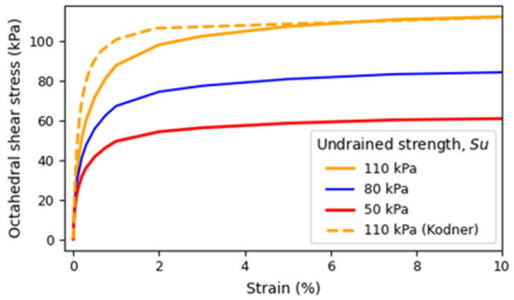

Figure 10. Stress–strain curves for the foundation soil, showing effects of reduced undrained strength (Su) and different stiffness degradation laws (Kondner vs. Vucetic & Dobry).

The input motion was applied as force history at the SSI model base and as surface acceleration in the fixed-base model. As a result of IMPL-EX materials, the solution always converges in two iterations. To control error build-up in the material solution the time step is decreased to the 1/4th of the seismic record sampling step.

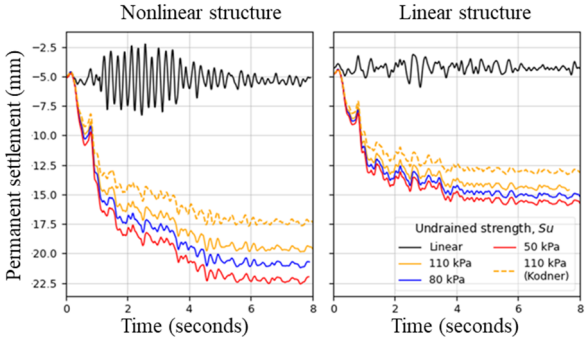

Figure 11. Computed settlements for different soil strengths and stiffness reduction rates; slower stiffness reduction causes greater settlements than Su reduction alone.

The settlement results in Figure 11 highlight the dual influence of undrained strength and stiffness degradation characteristics. As expected, reducing Su increases settlements; however, the dominant factor is the rate of stiffness reduction during shaking. The hyperbolic Kodner-type backbone, with its long initial linear segment followed by an abrupt stiffness drop, transmits more high-frequency energy to the tower in the early stages of motion than backbones that begin degrading stiffness immediately, such as the Vucetic–Dobry curves. This early high-frequency input accelerates structural response and settlement development. Consequently, the settlement magnitude is controlled more by the G/Gmax curve shape than by Su itself.

When the masonry tower is allowed to crack, settlements increase further. This is due to the reduction in confinement forces applied on the foundation soil by the foundation

masonry. The resulting increase in the soil stress-strain demand amplifies foundation rocking and toe contact pressures, driving ratcheting-type cyclic shear deformation in the foundation soil. Because the soil beneath the active toe deforms mainly in shear distortion, these cycles accumulate as permanent settlement without requiring large peak accelerations.

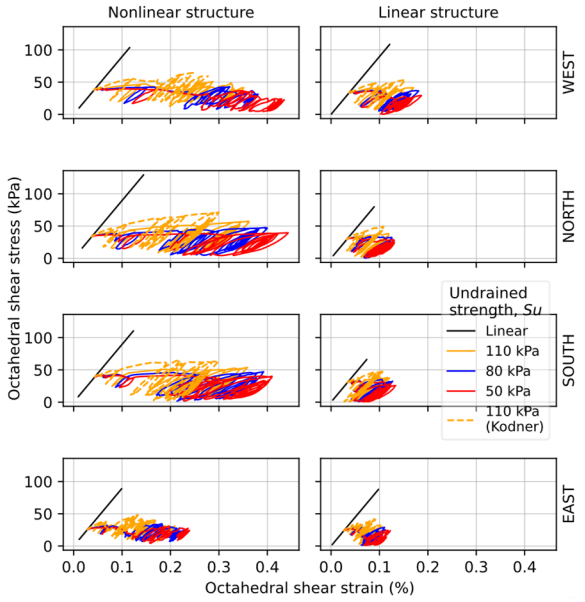

Figure 12. Soil stress–strain response for elastic and cracked structure cases; foundation softening and increased tower oscillations drive higher soil nonlinearity.

The stress–strain loops in Figure 12 confirms this mechanism. In the elastic superstructure case, shear strains around the foundation remain small and hysteresis loops narrow. Allowing the superstructure to crack produces much wider loops and higher peak strains, indicating stronger soil nonlinearity and greater energy dissipation at the foundation. This elevated nonlinearity results from the combination of softer post-cracking foundation response and the increased horizontal motion of the tower.

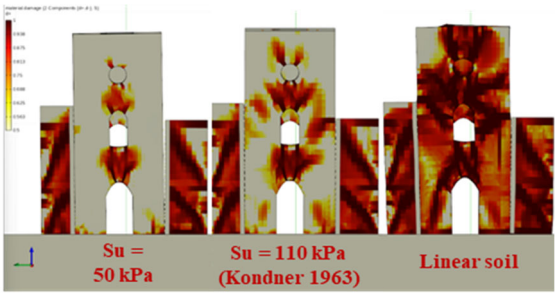

Figure 13. Cracking patterns versus soil stiffness; slower stiffness reduction transmits more high-frequency energy, increasing masonry damage severity.

The implications for structural damage are shown in Figure 13. Forcing the soil to remain linear produces the most severe cracking, as the foundation dissipates no energy and the full seismic demand is imposed on the tower. As Su decreases, more energy is absorbed in the foundation soil, generally reducing tower cracking. Yet, the governing control is again the stiffness degradation rate. A backbone with a long initial elastic range sustains higher stress capacity at small strains, enabling greater transmission of high-frequency accelerations before yielding. For brittle masonry, this means early-cycle cracking can occur before soil nonlinearity engages. Conversely, curves that begin degrading stiffness at small strains reduce high-frequency transmission earlier, limiting crack propagation.

In summary, the results demonstrate that while reducing foundation soil strength can help dissipate seismic energy and mitigate masonry cracking, the form of the stiffness degradation curve is the more critical parameter in controlling both foundation settlement and superstructure damage.

6 CONCLUSIONS

The foundation rotation in shallow-founded masonry towers is a dominant factor in determining the fundamental period of the soil–structure interaction (SSI) system. The shear modulus reduction characteristics of the foundation soil has a strong influence on the cracking damage observed in the tower. When the soil exhibits greater shear modulus reduction at small strain levels, the foundation dissipates more seismic energy, reducing the high-frequency accelerations transmitted to the superstructure and thereby mitigating cracking. Conversely, a slower stiffness reduction rate, even at the same undrained strength, allows more high-frequency energy to reach the tower before significant softening occurs—resulting in more intense cracking damage.

A novel and important finding of this study is that foundation softening caused by cracking can significantly increase settlements. As the foundation masonry accumulates damage, its stiffness is reduced, decreasing the confinement effect on foundation soil and increasing the overall compliance of the soil–foundation system. The resulting stress–strain response in the surrounding soil shows orders-of-magnitude larger nonlinear strains, which accelerate settlement accumulation. Thus, contrary to the conventional assumption that a softer foundation reduces demand on the superstructure, the interplay between foundation cracking and soil nonlinearity can lead to larger settlements, even when structural forces are partially mitigated.

The rocking isolation mechanism previously observed in shallow-founded reinforced concrete (RC) structures is also present in masonry towers, but with extended mechanics. While rocking can reduce superstructure forces, settlements can increase when foundation cracking occurs.

It is also worth noting that this study employs the IMPL-EX integration technique for solving the material constitutive equations, which often leads to prohibitive computational costs in large SSI models such as the one studied here. As shown, the IMPL-EX approach proved effective in capturing cyclic soil behavior while maintaining minimal computational overhead.

7 ACKNOWLEDGEMENTS

The work presented in this paper was carried out within the framework of the “Dipartimenti di Eccellenza” project, funded by the Italian Ministry of Education, University and Research at IUSS Pavia. The authors gratefully acknowledge Dr. Ali Güney Özcebe for his valuable technical insights on site response analysis and 3D geotechnical modelling in OpenSees for nonlinear dynamic analysis. This study forms part of the first author’s PhD research and is included in two journal papers, under review in parallel with this paper.

8 REFERENCES

Akan, O.D. 2024. 3D numerical investigation of nonlinear seismic soil-structure interaction in shallow-founded masonry towers with mixed implicit-explicit integration for improved solution stability. PhD Thesis. Scuola Universitaria Superiore IUSS Pavia.

Anastasopoulos, I., Gelagoti, F., Kourkoulis, R. and Gazetas, G. 2011. Simplified Constitutive Model for Simulation of Cyclic Response of Shallow Foundations: Validation against Laboratory Tests.

Journal of Geotechnical and Geoenvironmental Engineering 137(12), 1154–1168. https://doi.org/10.1061/(ASCE)GT.1943-5606.0000534.

Ancheta, T.D., Darragh, R.B., Stewart, J.P., Seyhan, E., Silva, W.J., Chiou, B.S.-J., Wooddell, K.E., Graves, R.W., Kottke, A.R., Boore, D.M., Kishida, T. and Donahue, J.L. 2014. NGA-West2 Database. Earthquake Spectra 30(3), 989–1005. https://doi.org/10.1193/070913EQS197M.

Boore, D.M., Stewart, J.P., Seyhan, E. and Atkinson, G.M. 2014. NGA-West2 Equations for Predicting PGA, PGV, and 5% Damped PSA for Shallow Crustal Earthquakes. Earthquake Spectra 30(3), 1057–1085. https://doi.org/10.1193/070113EQS184M.

Bray, J.D. and Macedo, J. 2017. 6th Ishihara lecture: Simplified procedure for estimating liquefaction-induced building settlement. Soil Dynamics and Earthquake Engineering 102(September), 215–231. https://doi.org/10.1016/j.soildyn.2017.08.026.

Bullock, Z., Karimi, Z., Dashti, S., Porter, K., Liel, A.B. and Franke, K.W. 2019. A physics-informed semi-empirical probabilistic model for the settlement of shallow-founded structures on liquefiable ground. Geotechnique 69(5), 406–419. https://doi.org/10.1680/jgeot.17.P.174.

Camata, G., Cifelli, L., Spacone, E., Conte, J. and Torrese, P. 2008. Safety analysis of the bell tower of St. Maria Maggiore cathedral in Guardiagrele (Italy). Proc. 14th World Conference on Earthquake Engineering. https://doi.org/10.4203/ccp.88.58.

Dashti, S., Bray, J.D., Pestana, J.M., Riemer, M. and Wilson, D. 2010. Centrifuge Testing to Evaluate and Mitigate Liquefaction-Induced Building Settlement Mechanisms. Journal of Geotechnical and Geoenvironmental Engineering 136(7), 918–929. https://doi.org/10.1061/(asce)gt.1943-5606.0000306.

Gazetas, G. 2015. 4th Ishihara lecture: Soil–foundation–structure systems beyond conventional seismic failure thresholds. Soil Dynamics and Earthquake Engineering 68, 23–39. https://doi.org/10.1016/j.soildyn.2014.09.012.

Gelagoti, F., Kourkoulis, R., Anastasopoulos, I. and Gazetas, G. 2012. Rocking isolation of low-rise frame structures founded on isolated footings. Earthquake Engineering & Structural Dynamics 41(7), 1177–1197.

Gu, Q., Conte, J.P., Yang, Z. and Elgamal, A. 2011. Consistent tangent moduli for multi-yield-surface J2 plasticity model. Computational Mechanics 48(1), 97–120. https://doi.org/10.1007/s00466-011-0576-7.

Guerrini, G., Senaldi, I., Scherini, S., Morganti, S., Magenes, G., Beyer, K. and Penna, A. 2017. Material Characterization for the Shaking-Table Test of the Scaled Prototype of a Stone Masonry Building Aggregate. ANIDIS. Pistoia.

Kastelic, V., Vannoli, P., Burrato, P., Fracassi, U., Tiberti, M.M. and Valensise, G. 2013. Seismogenic sources in the Adriatic Domain. Marine and Petroleum Geology 42, 191–213. https://doi.org/10.1016/j.marpetgeo.2012.08.002.

Kohrangi, M., Bazzurro, P., Vamvatsikos, D. and Spillatura, A. 2017. Conditional spectrum-based ground motion record selection using average spectral acceleration. Earthquake Engineering & Structural Dynamics 46(10), 1667–1685. https://doi.org/10.1002/eqe.2876.

Kondner, R.L. 1963. Hyperbolic Stress-Strain Response: Cohesive Soils. Journal of the Soil Mechanics and Foundations Division 89(1), 115–143. https://doi.org/10.1061/JSFEAQ.0000479.

Milani, G. and Clementi, F. 2021. Advanced Seismic Assessment of Four Masonry Bell Towers in Italy after Operational Modal Analysis (OMA) Identification. International Journal of Architectural Heritage 15(1), 157–186. https://doi.org/10.1080/15583058.2019.1697768.

Mróz, Z. 1967. On the description of anisotropic workhardening. Journal of the Mechanics and Physics of Solids 15(3), 163–175. https://doi.org/10.1016/0022-5096(67)90030-0.

Oliver, J., Huespe, A. E., and Cante, J. C. 2008. An implicit/explicit integration scheme to increase computability of non-linear material and contact/friction problems. Computer Methods in Applied Mechanics and Engineering 197(21–24), 1865–1889. https://doi.org/10.1016/j.cma.2007.11.027.

Ozsarac, V., Monteiro, R. and Calvi, G.M. 2023. Probabilistic seismic assessment of reinforced concrete bridges using simulated records. Structure and Infrastructure Engineering, 19(4) 554–574. https://doi.org/10.1080/15732479.2021.1956551.

Pelà, L., Cervera, M. and Roca, P. 2013. An orthotropic damage model for the analysis of masonry structures. Construction and Building Materials 41, 957–967. https://doi.org/10.1016/j.conbuildmat.2012.07.014.

Petracca, M., Camata, G., Spacone, E. and Pelà, L. 2022. Efficient Constitutive Model for Continuous Micro-Modeling of Masonry Structures. International Journal of Architectural Heritage 0(0), 1–13. https://doi.org/10.1080/15583058.2022.2124133.

Petracca, M., Candeloro, F. and Camata, G. 2017. Scientific Toolkit for OpenSees (STKO) user manual.

Prevost, J.H. 1989. DYNA1D: A computer program for nonlinear seismic site response analysis - technical documentation. Princeton, NJ: Princeton University.

Romero-Sánchez, E., Requena-Garcia-Cruz, M.-V. and Morales-Esteban, A. 2024. Impact of the soil-foundation-structure interaction in the seismic behaviour of a heritage masonry tower: The Giralda of Seville. Engineering Failure Analysis 163, p.108580. https://doi.org/10.1016/j.engfailanal.2024.108580.

Rosell, L.A. 2010. Explicit / Implicit Nonlinear Soil Structure Interaction Study of the Bell Tower of Santa Maria Maggiore , Guardiagrele. Istituto Universitario di Studi Superiori di Pavia.

Vucetic, M. and Dobry, R., 1991. Effect of Soil Plasticity on Cyclic Response. Journal of Geotechnical Engineering 117(1), 89–107. https://doi.org/10.1061/(ASCE)0733-9410(1991)117:1(89).

Whittaker, A., Atkinson, G., Baker, J., Bray, J., Grant, D., Hamburger, R., Haselton, C. and Somerville, P. 2011. Selecting and Scaling Earthquake Ground Motions for Performing Response-History Analyses. NIST.

Woessner, J., Laurentiu, D., Giardini, D., Crowley, H., Cotton, F., Grünthal, G., Valensise, G., Arvidsson, R., Basili, R., Demircioglu, M.B., Hiemer, S., Meletti, C., Musson, R.W., Rovida, A.N., Sesetyan, K., Stucchi, M., and The SHARE Consortium 2015. The 2013 European Seismic Hazard Model: key components and results. Bulletin of Earthquake Engineering 13(12), 3553–3596. https://doi.org/10.1007/s10518-015-9795-1.